Chemical Geology 443 (2016) 137–145

Contents lists available at ScienceDirect

Chemical Geology

journal homepage: www.elsevier.com/locate/chemgeo

First-principles phase diagram calculations for the carbonate quasibinary systems $CaCO_3$-$ZnCO_3$, $CdCO_3$-$ZnCO_3$, $CaCO_3$-$CdCO_3$ and $MgCO_3$-$ZnCO_3$

Z.T.Y. Liu [a], B.P. Burton [b], S.V. Khare [a,*], P. Sarin [c]

[a] Department of Physics and Astronomy, University of Toledo, Toledo, OH 43606, USA
[b] Materials Measurement Laboratory, Metallurgy Division, National Institute of Standards and Technology (NIST), Gaithersburg, MD 20899, USA
[c] School of Materials Science and Engineering, Oklahoma State University, Tulsa, OK 74106, USA

ARTICLE INFO

Article history:
Received 3 June 2016
Received in revised form 15 September 2016
Accepted 19 September 2016
Available online 21 September 2016

Keywords:
Density functional theory
Cluster expansion
Phase diagram
Calcite
Dolomite
Minrecordite

ABSTRACT

Quasibinary solid solutions of calcite-structure carbonate minerals play an important role in rock formation. We have investigated solid solutions with cations Ca^{2+}, Cd^{2+}, Mg^{2+} and Zn^{2+} by performing first-principles phase diagram calculations for $Ca_{1-x}Zn_xCO_3$, $Cd_{1-x}Zn_xCO_3$, $Ca_{1-x}Cd_xCO_3$ and $Mg_{1-x}Zn_xCO_3$ ($0 \le x \le 1$) with density functional theory, cluster expansion and Monte Carlo simulations. The end members and the dolomite structures were individually studied to analyze their structural parameters and bonding characteristics. Consolute temperatures and continuous order-disorder transition temperatures are 1450 K for $Ca_{1-x}Zn_xCO_3$ and 1000 K for $Cd_{1-x}Zn_xCO_3$, but below 100 K for $Ca_{1-x}Cd_xCO_3$ and $Mg_{1-x}Zn_xCO_3$. In agreement with existing literature, consolute temperatures increase with increasing differences in cation radii. If the dolomite structures are assumed to be stable, the phase diagram calculations predict that they persist to 1150 K for $Ca_{1-x}Zn_xCO_3$, and 900 K for $Cd_{1-x}Zn_xCO_3$ before decomposition at peritectoid points. This confirms the conjectured phase diagram for $Ca_{1-x}Zn_xCO_3$ in (Goldsmith, 1983. Rev. Mineral. Geochemistry 11). In addition, formation energies of the dolomite structures were decomposed into two parts: first a volume change, then chemical exchange and relaxation. They were compared with the corresponding random solid solutions at the same bulk compositions. (Meta)stability of the dolomite structures was demonstrated by this analysis, and was also studied by examining the bond lengths and cation octahedral distortions.

1. Introduction

Calcite, and its isotructural compounds are ubiquitous in the Earth's crust (Klein et al., 1993). Understanding them helps one evaluate rock-forming conditions and mining endeavors. Ca^{2+} in calcite is often mixed with other cations such as Mg^{2+}, Mn^{2+}, Fe^{2+}, Zn^{2+}, Co^{2+}, Ni^{2+}, Cu^{2+}, Pb^{2+}, Cd^{2+} to form solid solutions like $Ca_{1-x}Cd_xCO_3$ ($0 \le x \le 1$) and intermediate compounds such as dolomite $CaMg(CO_3)_2$. In addition, solid solutions and intermediate compounds can also form without Ca^{2+}, such as $Mg_{1-x}Zn_xCO_3$, and dolomite-structure $CdMg(CO_3)_2$. The chemistry of the calcite-structure carbonates influences the distribution and transport of those cations in sedimentary rocks and geofluids. Extensive experimental studies have been done on a few systems (Anovitz and Essene, 1987; Birch, 1983; Boni et al., 2011; Capobianco et al., 1987; de Capitani and Peters, 1981; Goldsmith and Graf, 1960, 1958; Goldsmith and Northrop, 1965; Goldsmith et al., 1962; Goldsmith, 1983, 1972; Khan and Barber, 1990; Mondillo et al., 2011; Navrotsky and Capobianco, 1987; Powell et al., 1984; Rosenberg and Champness, 1989; Rosenberg and Foit, 1979; Rosenberg, 1967, 1963a, 1963b), and the mixing behaviors have been studied through phase diagram calculations with a variety of methods. Empirical potential models and parameters (Purton et al., 2006) were used to perform direct Monte Carlo simulations (Binder and Heermann, 1988; Dunweg and Landau, 1993; Kohan et al., 1998; Laradji et al., 1995; Newman and Barkema, 1999) on systems such as $Ca_{1-x}Cd_xCO_3$ (Wang and de Leeuw, 2008), $Ca_{1-x}Mn_xCO_3$ (Wang et al., 2011) and $Ca_{1-x}Zn_xCO_3$ (Liu et al., 2015). The cluster expansion (CE) formalism (Connolly and Williams, 1983; De Fontaine, 1994; Ducastelle, 1991; Laks et al., 1992; Sanchez et al., 1984; Zunger, 1994) allows one to fit a series-type Hamiltonian to the formation energy values of a few supercell configurations as a set of effective cluster interactions (ECIs), pairs, triplets, quadruplets, and higher n-tuplets to allow faster energy evaluation. The energy to be fitted can be calculated with empirical potentials or electronic structure methods such as density functional theory (DFT) as demonstrated for alloys (Barabash et al., 2009; Chen et al., 2015; Gao et al., 2013; Ghosh et al., 2008; Liu and Zunger, 2009; Liu et al., 2005; Ravi et al., 2012; van de Walle et al., 2004), semiconductors (Burton et al., 2011, 2006; Kumagai et al., 2012; Li et al., 2015; Usanmaz et al., 2015; Xue et al., 2014), ionic compounds (Burton and van de Walle, 2012a, 2012b, 2006; Burton et al., 2012), and minerals including carbonates (Burton and van de Walle, 2003; Vinograd et al., 2009, 2007, 2006).

* Correspondence author.
E-mail address: sanjay.khare@utoledo.edu (S.V. Khare).

http://dx.doi.org/10.1016/j.chemgeo.2016.09.024
0009-2541/

With cations Mg^{2+} and Ca^{2+} in Group 2, Zn^{2+} and Cd^{2+} in Group 12, six $M^A_{1-x}M^B_xCO_3$ ($0 \le x \le 1$, M^A and M^B being different cations) solid solution systems can be derived. Burton and van de Walle (Burton and van de Walle, 2003) studied $Ca_{1-x}Mg_xCO_3$ and $Cd_{1-x}Mg_xCO_3$ with first-principles total energy cluster expansion and Monte Carlo simulations to generate the phase diagrams. Each system features two-phase fields up to ~1000 K, between the end members and the dolomite-structure intermediate phase, plus a continuous order-disorder transition at higher temperatures, which connect tricritical points at the maxima of the two-phase fields. In this work, we study phase relations of the other four systems $Ca_{1-x}Zn_xCO_3$, $Cd_{1-x}Zn_xCO_3$, $Ca_{1-x}Cd_xCO_3$ and $Mg_{1-x}Zn_xCO_3$. The radius of Zn^{2+} (0.74 Å) is similar to that of Mg^{2+} (0.72 Å), and so is Cd^{2+} (0.95 Å) to Ca^{2+} (1.00 Å). Therefore, we expect $Ca_{1-x}Zn_xCO_3$ and $Cd_{1-x}Zn_xCO_3$ to behave similarly to the previous two systems, while $Ca_{1-x}Cd_xCO_3$ and $Mg_{1-x}Zn_xCO_3$ should have very shallow miscibility gaps.

The most common intermediate compound derived from calcite is dolomite $CaMg(CO_3)_2$ because of Mg's abundance in the Earth's crust and dolomite's energetic favorability relative to calcite and magnesite. Mn^{2+} and Fe^{2+} often substitute for Mg^{2+} in dolomite, because of their similar cation radii. However, unlike $CaMg(CO_3)_2$ or $CaMn(CO_3)_2$, dolomite-structure $CaFe(CO_3)_2$ is apparently metastable (Goldsmith and Northrop, 1965). Instead, Fe^{2+} substitutes for Mg^{2+} up to 70 at.% but not beyond (Rosenberg, 1967). Similarly, Zn^{2+} substitutes for Mg^{2+}. Supergene metal-carrying and oxygen-rich meteoric fluids react with preexisting dolomite bodies that host Zn sulfide ores, replacing Mg^{2+} with Zn^{2+} to create Zn-dolomite. The incorporation of Zn^{2+} can be as high as 92 at.%, but the fully substituted dolomite-structure $CaZn(CO_3)_2$, minrecordite, is probably metastable (Boni et al., 2011; Rosenberg and Champness, 1989). In the vicinity of Zn-ores, continuous solution $Mg_{1-x}Zn_xCO_3$ can also be found. Here, we aim to obtain a deeper understanding of the energetics of ordering and/or phase separation in calcite-structure solid solutions. We compare known experimental results with our computations, and extend the discussion to Cd-related systems $Cd_{1-x}Zn_xCO_3$ and $Ca_{1-x}Cd_xCO_3$. We then analyze the (meta)stability of dolomite structures by decomposing mixing energies into two contributions: first a volume change, then chemical exchange and relaxation; and by examining the bond lengths and cation octahedral distortions. Specifically, we evaluate the energetic metastability of dolomite-structure $CaZn(CO_3)_2$ at different temperatures and estimate the temperature-upper-bound of highly substituted Zn-dolomites.

This study only considers quasibinaries, meaning that the system is assumed to obey a binary Gibbs phase rule with one free composition variable. We also ignore orientational order-disorder of the anion groups CO_3^{2-} as previously assumed (Burton and van de Walle, 2003; Vinograd et al., 2007).

2. Computational methods

We performed ab initio DFT computations using the Vienna Abinitio Simulation Package (VASP) (Kresse and Furthmuller, 1996a, 1996b; Kresse and Hafner, 1994, 1993) with the projector-augmented wave method (PAW) (Blöchl, 1994; Kresse and Joubert, 1999) and Purdew–Burke–Ernzerhoff (PBE) generalized gradient approximation (GGA) (Perdew et al., 1993, 1992). We selected the potentials of Ca_sv, Cd, Mg, Zn, C and O, where "_sv" denotes that the semi-core 3s and 3p electrons of Ca are also included. The plane wave energy cutoff was 520 eV to ensure correct cell volume and shape relaxations. The k-point meshes were created with k-points per reciprocal atom (KPPRA) of 1000, leading to an error of ~0.2 meV/atom in energy from a convergence test. Gaussian smearing was used with a sigma value as small as 0.05 eV. The convergence criterion was set to 10^{-5} eV in energy during the electronic iterations. For structural optimization, the cell volume, shape and atomic positions were allowed to relax until stress was minimized and force on any atom was below 0.02 eV/Å. This leads to an error of ~0.4 meV/atom.

To obtain equations of state (EOS's) of the calcite-structure end members $CaCO_3$, $CdCO_3$, $MgCO_3$ and $ZnCO_3$ and their dolomite structures, we picked 5 volume points in each case covering the equilibrium volume, fitted the total energies to the Birch-Murnaghan EOS (Birch, 1947), and derived equilibrium volumes, energies and bulk moduli (Liu et al., 2014a, 2014b, 2014c).

Energy landscapes, cluster expansions and phase diagrams were generated for systems $Ca_{1-x}Zn_xCO_3$, $Cd_{1-x}Zn_xCO_3$, $Ca_{1-x}Cd_xCO_3$ and $Mg_{1-x}Zn_xCO_3$ using the Alloy Theoretic Automated Toolkit (ATAT) (van de Walle and Asta, 2002; van de Walle and Ceder, 2002a; van de Walle, 2009; van de Walle et al., 2002). The MIT Ab-initio Phase Stability (maps) (van de Walle, 2009; van de Walle et al., 2002) code in ATAT was used to generate energy landscapes and CEs (details in Supplementary material). With well-converged CEs, the Easy Monte Carlo Code (emc2 and phb) (van de Walle and Asta, 2002; van de Walle and Ceder, 2002a) in ATAT was used to perform Monte Carlo (MC) simulations to obtain phase diagrams. A MC simulation box of $8 \times 8 \times 8$ 10-atom trigonal cells (1024 exchangeable sites) was chosen. We used semi-grand canonical (SGC) ensemble simulations, where one controls the chemical potential (μ) and temperature (T). The chemical potential is defined as $\mu_i = \left(\partial G / \partial n_i\right)_{T,n_{j\neq i}}$, where G is the Gibbs free energy, n_i is the number of atoms of species i in the simulation cell. In a binary system $A_{1-x}B_x$, $\mu = \mu_A - \mu_B$ is used as the input. Most of the phase boundaries were obtained by identifying abrupt changes in bulk composition and/or long-range order scanning through μ and T axes. Long-range order is defined here as the occupancy of each exchangeable site relative to its value in the given starting ground state. For each μ and T point, sufficient MC passes were used to equilibrate and average the system to reach a composition precision of 0.01. The canonical ensemble simulations were also performed where one controls the composition (x) and T to track the transition/disordering temperature of the dolomite-structure phase. For each temperature point, 1500 MC passes were used to average thermodynamic quantities, and 1500 passes to re-equilibrate the system after the phase transition.

We also included vibrational free energy contributions (van de Walle and Ceder, 2002b; van de Walle, 2013, 2009; Wang et al., 2016) to the phase diagrams. There were large variations (200 K) in the resultant consolute and transition temperatures depending on the numbers of structures included in the calculation of bond stiffness vs bond length relations. Therefore we present those results in the Supplementary material.

3. Results and discussion

3.1. Cell parameters of the end members and dolomite structures

Table 1 lists the lattice parameters of the 10-atom trigonal cell used in calculations of calcite-structure $CaCO_3$, $CdCO_3$, $MgCO_3$, $ZnCO_3$ and dolomite structures. The prototype structure is described in Table S1 of the Supplementary material. Lattice parameters of the 30-atom hexagonal cell are also given for ease of comparison in Table 1. These values compare well with experimental results from Graf (Graf, 1961), with a small and consistent overestimation due to the use of GGA in our DFT calculations (Liu et al., 2014a, 2014b, 2014c). The formula unit (f.u.) contains 5 atoms. Formation energies (ΔE_f) are defined with respect to the two end members,

$$\Delta E_f\left(M^A_{1-x}M^B_xCO_3\right) = E\left(M^A_{1-x}M^B_xCO_3\right) - (1-x)E\left(M^ACO_3\right) - xE\left(M^BCO_3\right) \quad (1)$$

There are numerous reference values from the literature for ΔE_f of the dolomite-structure $CaMg(CO_3)_2$ and $CdMg(CO_3)_2$. For $CaMg(CO_3)_2$,

Table 1
Lattice paramters of the trigonal and hexagonal unit cells, volumes per formula unit (V/f.u.), total energies per formula unit (E/f.u.), formation energies per formula unit (ΔE_f/f.u.) with respect to calcite-structure end members, and bulk moduli (B) of $CaCO_3$, $CdCO_3$, $MgCO_3$, $ZnCO_3$ and the six dolomite structures. The formula unit is MCO_3 and values corresponding to dolomite structures have reduced formula ½ $M^AM^B(CO_3)_2$. The trigonal cell contains 2 formula units, while the hexagonal cell contains 6. Unless specified, values were obtained from PAW-PBE calculations.

	a (Å)	α (°)	a_{hex} (Å)	c_{hex} (Å)	V/f.u. (Å^3)	E/f.u. (eV)	E_f/f.u. (eV)	B (GPa)
$CaCO_3$	6.45	46.10	5.05	17.27	63.7	−37.374		67.1
Ref.[a]	6.375	46.08	4.990	17.061	61.3			67[b]
$CdCO_3$	6.27	47.06	5.00	16.69	60.3	−31.549		84.2
Ref.[a]	6.131	47.32	4.920	16.298	57.0			97[b]
$MgCO_3$	5.75	48.06	4.68	15.23	48.2	−35.779		105.2
Ref.[a]	5.675	48.18	4.633	15.016	46.5			107[b]
$ZnCO_3$	5.78	48.14	4.72	15.30	49.2	−32.196		111.7
Ref.[a]	5.683	48.33	4.652	15.025	46.9			124[b]
$CaMg(CO_3)_2$	6.09	47.03	4.86	16.22	55.3	−36.597	−0.021	85.7
Ref.[a]	6.015	47.11	4.807	16.010	53.4		−0.060(3)[c] −0.034[e] −0.038[f] −0.040[g]	
$CdMg(CO_3)_2$	5.98	47.75	4.84	15.85	53.5	−33.691	−0.027	88.6
Ref.[a]	5.90	47.78	4.777	15.641	51.5		−0.029(4)[d] −0.050[f]	
$CaZn(CO_3)_2$	6.14	46.77	4.87	16.36	56.0	−34.780	0.005	89.6
$CdZn(CO_3)_2$	6.01	47.56	4.85	15.97	54.2	−31.872	0.000	92.1
$CaCd(CO_3)_2$	6.34	46.72	5.03	16.92	61.8	−34.466	−0.004	74.1
$MgZn(CO_3)_2$	5.76	48.15	4.70	15.25	48.7	−33.993	−0.005	108.0

[a] Experimental values of a, α, a_{hex}, c_{hex} and V (Graf, 1961).
[b] Experimental (Zhang and Reeder, 1999).
[c] Experimental (Navrotsky and Capobianco, 1987).
[d] Experimental (Capobianco et al., 1987).
[e] PAW-LDA (this work).
[f] USPP-LDA (Burton and van de Walle, 2003).
[g] Empirical potentials (Vinograd et al., 2007).

we observe that our PAW-PBE value of −0.021 eV/f.u. is less negative (structure less stable) than one experimental value of −0.060 eV/f.u. (Navrotsky and Capobianco, 1987), or the USPP-LDA (ultrasoft pseudopotential-local density approximation) value of −0.038 eV/f.u. (Burton and van de Walle, 2003), or that with empirical potentials of −0.040 eV/f.u. (Vinograd et al., 2007). To confirm that it is due to the use of GGA potentials, we performed calculations with PAW-LDA, and obtained very similar result −0.034 eV/f.u. as the USPP-LDA value mentioned above. For $CdMg(CO_3)_2$, our PAW-PBE value of −0.027 eV/f.u. is very close to the experimental value of −0.029 eV/f.u. (Capobianco et al., 1987), but the USPP-LDA value of −0.050 eV/f.u. (Burton and van de Walle, 2003) is much more negative. The deviations are within expected variations in state-of-the-art theoretical methods.

Bulk moduli (B) obtained from the EOS's fitting show a small and consistent GGA underestimation relative to experimental values from Zhang and Reeder (Zhang and Reeder, 1999) as expected with this approximation.

3.2. Formation energy landscapes and cluster expansions

Fig. 1 shows formation energies as functions of bulk composition for of $Ca_{1-x}Zn_xCO_3$, $Cd_{1-x}Zn_xCO_3$, $Ca_{1-x}Cd_xCO_3$ and $Mg_{1-x}Zn_xCO_3$. The behavior of these four systems can be divided into two groups: the first group $Ca_{1-x}Zn_xCO_3$ and $Cd_{1-x}Zn_xCO_3$ has large differences in cation radii, resulting in positive ΔE_f for most structures; the second group, $Ca_{1-x}Cd_xCO_3$ and $Mg_{1-x}Zn_xCO_3$ has small differences in cation radii, and many more members with negative ΔE_f, although the energy scale is of order ~5 meV/f.u., more than an order of magnitude smaller than the first group, ~100 meV/f.u.

Fig. 2 and Table 2 summarize the numbers of structures calculated with DFT, numbers of clusters, fitted ECIs and cross validation (CV) scores. Detailed information of the cluster sets is provided in Table S2 of the Supplementary material. Similar to what was observed in other carbonate systems, such as $Ca_{1-x}Mg_xCO_3$ and $Cd_{1-x}Mg_xCO_3$ (Burton and van de Walle, 2003), the inter-layer nearest-neighbor (nn) ECI is positive, while the intra-layer nn ECI is negative, facilitating stabilizing the dolomite structure. In addition, the ECI trends of $Ca_{1-x}Zn_xCO_3$ and $Cd_{1-x}Zn_xCO_3$ are very similar, with the energy scale of $Ca_{1-x}Zn_xCO_3$ larger than that of $Cd_{1-x}Zn_xCO_3$.

Observing the DFT-calculated structures in Fig. 1, the agreement with CE-fitted values is satisfactory. The CV scores in Table 2 are larger for $Ca_{1-x}Zn_xCO_3$ and $Cd_{1-x}Zn_xCO_3$ than for $Ca_{1-x}Cd_xCO_3$ and $Mg_{1-x}Zn_xCO_3$, because the overall energy values are larger. The fitting is less satisfactory for the latter two because ΔE_f values of their structures are at the limits of DFT precision. In Section 2 we mentioned the numerical errors of the k-point meshes and cell parameter optimization are ~0.2 and ~0.4 meV/atom, contributing to ~2 meV/f.u., comparable to their energy scales. However, all phases here have closely related crystal structures, which implies an order of magnitude greater precision owing to error cancellation.

Ground-state analysis was performed by enumeration of all 136,026 symmetrically inequivalent structures with 16 or fewer exchangeable sites per supercell. This number differs from a simple geometric series $\sum_{n=1}^{8}(2^2)^n = 87{,}380$ (2 exchangeable sites in a primitive trigonal unit cell) because there is more than one 10-, 20-, .0.80-atom supercell, and because some structures are identical. ΔE_f of the dolomite structure is slightly above the convex hull in $Ca_{1-x}Zn_xCO_3$ (5 meV/f.u.), and just below 0 in $Cd_{1-x}Zn_xCO_3$ (−0.5 meV/f.u.). All other non-end-member structures have positive ΔE_f. In each of Fig. 1(a) and (b), between the end members and the dolomite structure, the energy values form two arches, suggesting regions of immiscibility. In $Ca_{1-x}Cd_xCO_3$ and $Mg_{1-x}Zn_xCO_3$ some have $\Delta E_f < 0$. ΔE_f of both dolomite structures are below 0, and there are more structure energies on the convex hull in $Ca_{1-x}Cd_xCO_3$.

We also evaluated ΔE_f of configurations with correlations corresponding to random solid solutions (van de Walle et al., 2013) at different compositions, and fitted them to a smooth curve for each system. As expected, the curves appear up-bowing (concave) for systems $Ca_{1-x}Zn_xCO_3$ and $Cd_{1-x}Zn_xCO_3$, close to 0 for $Ca_{1-x}Cd_xCO_3$ and slightly down-bowing (convex) for $Mg_{1-x}Zn_xCO_3$.

3.3. Phase diagrams

Fig. 3 shows the calculated phase diagrams and Table 3 lists consolute, peritectoid and transition temperatures. The systems $Ca_{1-x}Zn_xCO_3$ and $Cd_{1-x}Zn_xCO_3$ both have miscibility gaps at high temperature, 1450 K and 1000 K respectively. The phase boundaries between the Ca(Cd)-rich side and Zn-rich side are asymmetric, leaning towards the carbonate with the smaller cation, Zn^{2+}. This phenomenon was also observed for other carbonate systems (Goldsmith, 1983), $Ca_{1-x}Mg_xCO_3$ and $Cd_{1-x}Mg_xCO_3$ (Burton and van de Walle, 2003; Vinograd et al., 2007), and transition metal carbide systems $Ti_{1-x}Zr_xC$ and $Ti_{1-x}Hf_xC$ (Adjaoud et al., 2009). The phase boundaries for $Ca_{1-x}Zn_xCO_3$ are in agreement with the scarce high-temperature experimental data (Goldsmith and Northrop, 1965). At low temperatures, both experiments and our computation show that the incorporation of Zn^{2+} into the Ca-rich side is minimal (Lamble et al., 1997; Reeder et al., 1999; Tsusue and Holland, 1966). Both the outlines of the miscibility gap in $Ca_{1-x}Cd_xCO_3$ and the

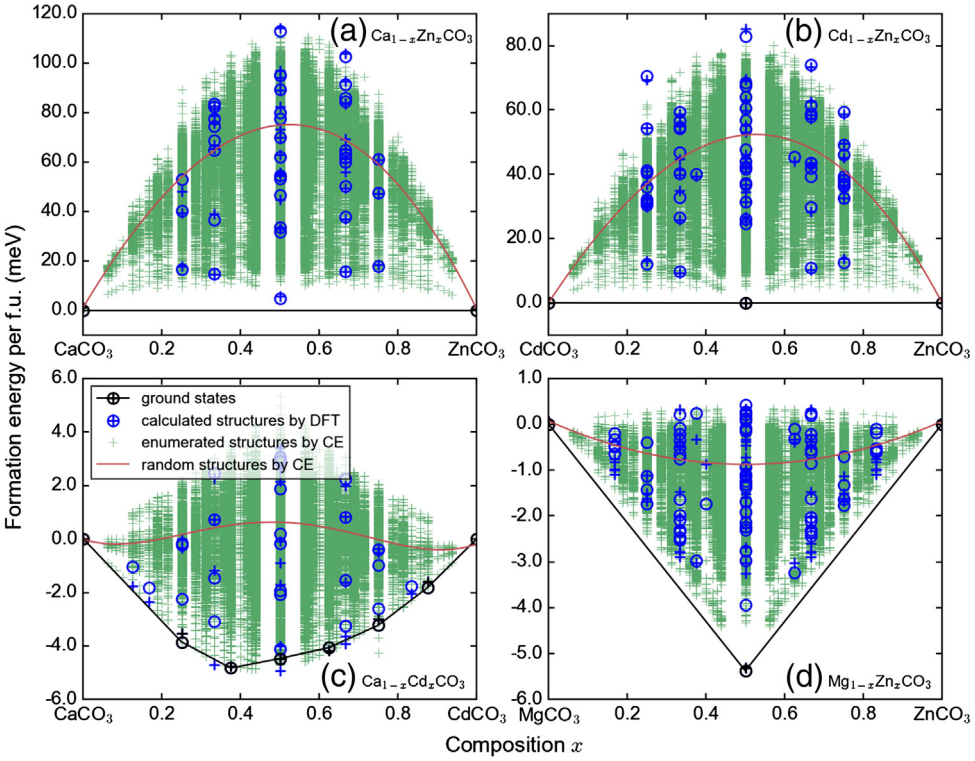

Fig. 1. Formation energy landscapes of (a) $Ca_{1-x}Zn_xCO_3$, (b) $Cd_{1-x}Zn_xCO_3$, (c) $Ca_{1-x}Cd_xCO_3$ and (d) $Mg_{1-x}Zn_xCO_3$. Energy values are per formula unit, i.e. per exchangeable site. Black markers and convex hull lines stand for ground states, and blue markers stand for the structures calculated with DFT and used to obtain the cluster expansions (CEs). Green crosses stand for a 16-exchangeable-site ground-state analysis. Among the markers, hollow circles stand for DFT values, and crosses stand for CE-fitted values. Red curves stand for CE-fitted values of random solid solution configurations. (For interpretation of the references to colour in this figure legend, the reader is referred to the web version of this article.)

continuous order-disorder transition line of the dolomite-structure phase in $Mg_{1-x}Zn_xCO_3$ close at ~100 K. Note that $Ca_{1-x}Cd_xCO_3$ took a long simulation-time to equilibrate all the multiple ground states, so we did more detailed SGC ensemble simulations at different temperature points and observed the abrupt changes in x with respect to μ in Fig. 3(e). The disappearance of these abrupt changes and the smoothing of the curves suggest closing of the miscibility gap. Wang and de Leeuw (Wang and de Leeuw, 2008) did thermodynamic simulations with empirical potentials and calculated a consolute temperature of 200 K, although their convex hull only has the two end members with an up-bowing ΔE_f curve of ~10 meV/f.u. (estimated from their figure). We note that these energy

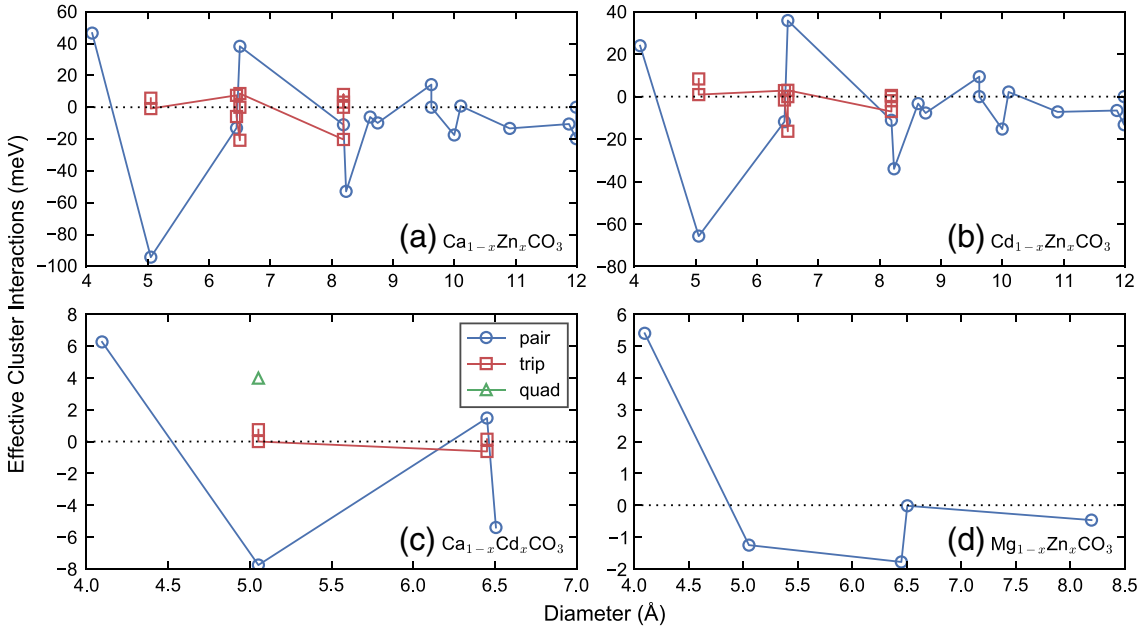

Fig. 2. Effective cluster interactions (ECIs) of (a) $Ca_{1-x}Zn_xCO_3$, (b) $Cd_{1-x}Zn_xCO_3$, (c) $Ca_{1-x}Cd_xCO_3$ and (d) $Mg_{1-x}Zn_xCO_3$. ECI values have been multiplied by their multiplicities. Blue circles, red squares and green triangles stand for pair, triplet and quadruplet interactions. Connecting lines are a guide to the eye. (For interpretation of the references to colour in this figure legend, the reader is referred to the web version of this article.)

Table 2
Numbers of structures calculated with DFT, numbers of clusters in pairs, triplets and quadruplets, and cross-validation (CV) scores of $Ca_{1-x}Zn_xCO_3$, $Cd_{1-x}Zn_xCO_3$, $Ca_{1-x}Cd_xCO_3$ and $Mg_{1-x}Zn_xCO_3$.

	Num. of structures	Num. of clusters (pair + trip + quad)	CV score (meV)
$Ca_{1-x}Zn_xCO_3$	42	16 + 11	6.2
$Cd_{1-x}Zn_xCO_3$	60	16 + 11	2.4
$Ca_{1-x}Cd_xCO_3$	42	4 + 4 + 1	0.6
$Mg_{1-x}Zn_xCO_3$	78	5	0.4

Table 3
Consolute temperatures (T_C), peritectoid points (T_P) and dolomite order-disorder transition temperatures (T_{trans}) of $Ca_{1-x}Zn_xCO_3$, $Cd_{1-x}Zn_xCO_3$, $Ca_{1-x}Cd_xCO_3$ and $Mg_{1-x}Zn_xCO_3$.

	T_C (K)	T_P (K)	T_{trans} (K)
$Ca_{1-x}Zn_xCO_3$	1450	1150	
$Cd_{1-x}Zn_xCO_3$	1000	900	
$Ca_{1-x}Cd_xCO_3$	<100		
$Mg_{1-x}Zn_xCO_3$			<100

values are small and different modeling methods give different results, but the low-T miscibility gaps are apparent in both cases. For $Mg_{1-x}Zn_xCO_3$, the complete miscibility above 100 K matches both geochemical observations and experimental studies (Mondillo et al., 2011; Rosenberg and Champness, 1989).

The dolomite structures introduce another metastable state to the phase diagrams of systems $Ca_{1-x}Zn_xCO_3$ and $Cd_{1-x}Zn_xCO_3$. In $Ca_{1-x}Zn_xCO_3$ ΔE_f of the dolomite structure is 5 meV/f.u., and in $Cd_{1-x}Zn_xCO_3$ it is only −0.1 meV/f.u., within DFT uncertainty. With $\Delta E_f \le 0$ the dolomite structure is stable, and with $\Delta E_f > 0$ it is metastable relative to the two end members. The energy landscapes of these two systems in Fig. 1(a)(b) show two arches across the end members and the dolomite structure, suggesting immiscibility. The transition temperature of the dolomite-structure phase scales with the energy difference between its ΔE_f and that of the corresponding disordered state. Therefore, if the dolomite structure is assumed to be stable relative to the end members, its single-phase field persists up to a high transition temperature. This was confirmed by our SCG ensemble and canonical ensemble simulations, taking the dolomite structure as a member of the ground states. In both simulations, we obtained similar transition temperatures. Fig. 4 shows the long-range order abruptly dropping to 0.5 for the two systems, marking the transition temperatures of the dolomite-structure phases. They are 1150 K for $Ca_{1-x}Zn_xCO_3$ and 900 K for $Cd_{1-x}Zn_xCO_3$. The dolomite-structure phase is not stable enough to split and exceed the miscibility gap. Instead, as its long-range order sharply drops, phase separation is more energetically favorable. Therefore, continuous order-disorder transition line, like what we've seen in $Mg_{1-x}Zn_xCO_3$ in Fig. 3(d), and $Ca_{1-x}Mg_xCO_3$ and $Cd_{1-x}Mg_xCO_3$ (Burton and van de Walle, 2003), becomes a peritectoid point. In addition, the dolomite-structure single-phase field is extremely narrow in composition, because a stoichiometric and highly ordered configuration is needed to maintain its relative energetic advantage below the peritectoid point.

As indicated by the positive ΔE_f, this dolomite-structure $CaZn(CO_3)_2$, minrecordite, is metastable. However, extensive (92 at.%) substitution of Zn^{2+} for Mg^{2+} in dolomite $CaMg(CO_3)_2$ is possible. The chemical stability of this near-end solid solution should be similar to minrecordite. As predicted by our computation, $CaZn(CO_3)_2$ decomposes above 1150 K. This confirms the conjectured phase diagram by Goldsmith

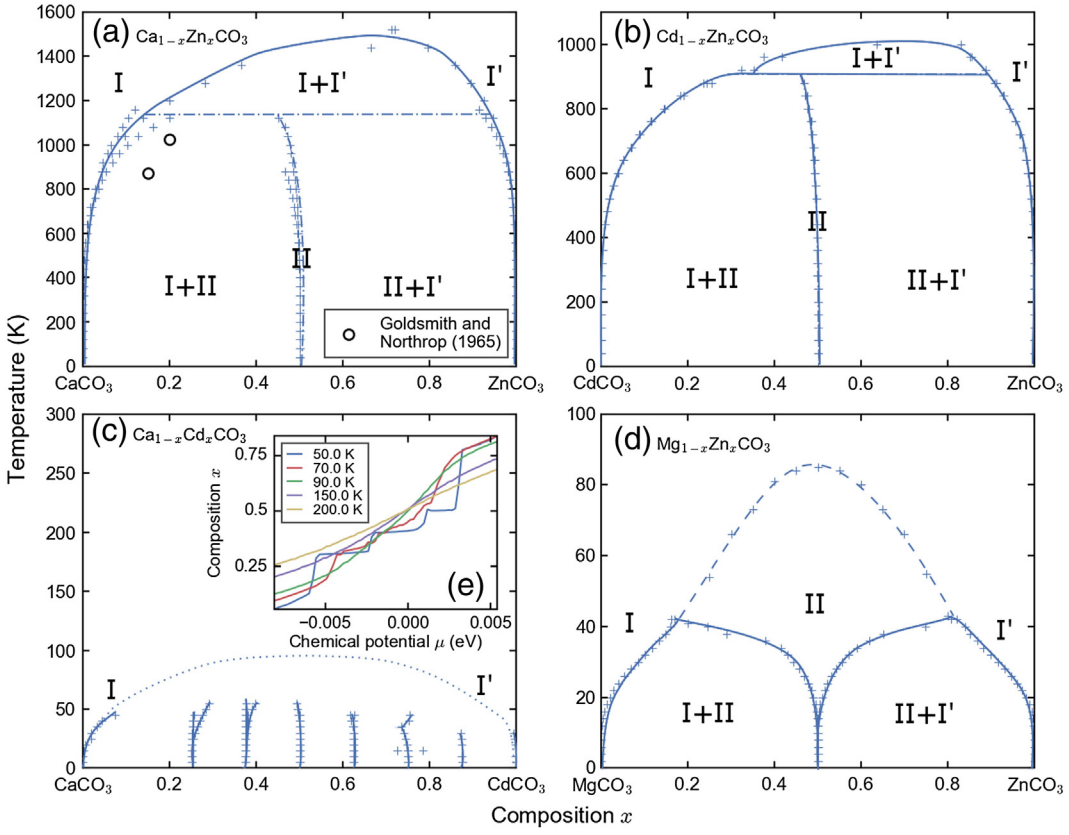

Fig. 3. Calculated phase diagrams of (a) $Ca_{1-x}Zn_xCO_3$, (b) $Cd_{1-x}Zn_xCO_3$, (c) $Ca_{1-x}Cd_xCO_3$ and (d) $Mg_{1-x}Zn_xCO_3$. Crosses are the raw data points, and curves are interpolations and extrapolations. In (a), dash-dotted curves stand for influence of the dolomite structure on the topology of the phase diagram. Hollow circles are experimental data points. In (c), the dotted curve stands for the estimated consolute boundary, as demonstrated by the inset (e). In (d), the dashed curve stands for the continuous order-disorder transition points. In all 4 subfigures, calcite-structure phases are labeled as I and I′, and dolomite-structure phases as II. In (e), curves stand for compositions with respect to chemical potentials at various temperatures in a semi-grand-canonical ensemble simulation.

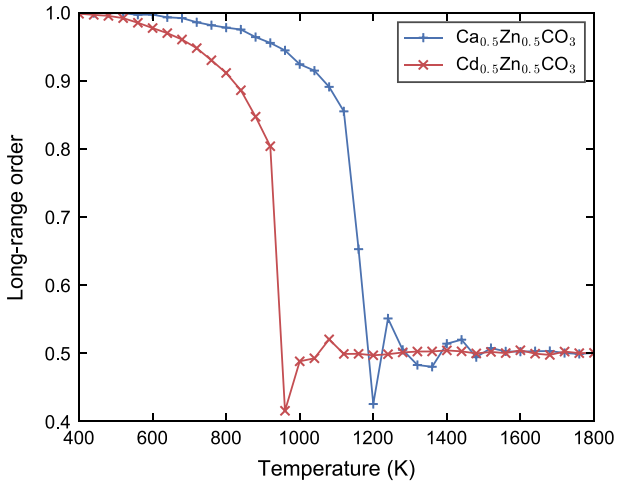

Fig. 4. Long-range order as a function of temperature for $Ca_{0.5}Zn_{0.5}CO_3$ and $Cd_{0.5}Zn_{0.5}CO_3$ in canonical ensemble simulations. The onsets of the abrupt drops to 0.5 mark the transition temperatures of the dolomite-structure phases.

(Goldsmith, 1983), where the estimated maximum thermal instability is 600 °C (Goldsmith, 1983; Rosenberg and Champness, 1989). Such agreement demonstrates the effectiveness of our simulation method with DFT, CE and MC, and serves as a good prediction for the similar case $CdZn(CO_3)_2$, where experimental data are lacking. ΔE_f of this dolomite structure is negative and very close to zero. It should either be stable at low temperatures, or can be approached from $CdMg(CO_3)_2$ via cation substitution up to >90 at.%. The 900 K instability temperature will not impede its formation in geochemical environments, because the precipitation temperature is similar to the temperature of meteoric fluids during the main weathering periods, within 11–23 °C (Boni et al., 2011; Gilg et al., 2008).

3.4. Random solid solutions

We also performed CE for the molar volumes, and calculated the composition dependent volume deviations from linearity for random solid solutions shown in Fig. 5, defined as:

$$V_{\text{linear}} = (1-x)V_{M^ACO_3} + xV_{M^BCO_3},$$

$$\text{Volume deviation of } M^A_{1-x}M^B_xCO_3 \equiv \frac{\left[V_{M^A_{1-x}M^B_xCO_3} - V_{\text{linear}}\right]}{V_{\text{linear}}}. \quad (2)$$

We can see that in all six systems, the random solid solutions have small negative deviations, below 1%. Deviations for the dolomite structure volumes are also tabulated, and they are generally more negative than their random solid solution counterparts.

We separated the solid solution mixing into two steps, volume change (vc) and chemical exchange and relaxation (xc-rlx), and observe the energy changes with respect to the end members. The two energy changes are defined as:

$$\Delta E_{vc}\left(M^A_{1-x}M^B_xCO_3\right) = (1-x)\left[E_{M^ACO_3}\left(V_{M^A_{1-x}M^B_xCO_3}\right) - E_{M^ACO_3}\left(V_{M^ACO_3}\right)\right] + x\left[E_{M^BCO_3}\left(V_{M^A_{1-x}M^B_xCO_3}\right) - E_{M^BCO_3}\left(V_{M^BCO_3}\right)\right],$$

$$\Delta E_{xc-rlx}\left(M^A_{1-x}M^B_xCO_3\right) = E\left(M^A_{1-x}M^B_xCO_3\right) - (1-x)E_{M^ACO_3}\left(V_{M^A_{1-x}M^B_xCO_3}\right) - xE_{M^BCO_3}\left(V_{M^A_{1-x}M^B_xCO_3}\right),$$

$$\Delta E_f = \Delta E_{vc} + \Delta E_{xc-rlx}, \quad (3)$$

where $E_{M^ACO_3}$ and $E_{M^BCO_3}$ denote energies depending on the EOS's of the two end members M^ACO_3 and M^BCO_3. ΔE_{vc} evaluates the energy change from expansion/contraction of the end member structures to the volume of the solid solution, while ΔE_{xc-rlx} measures the effect of chemical exchange, solution cell shape and atomic position relaxation.

Fig. 6 shows ΔE_{vc} and ΔE_{xc-rlx} of random solid solutions and the dolomite structures. The energy scale is larger than that of ΔE_f, and a large part of ΔE_{vc} is canceled out by ΔE_{xc-rlx}, leading to ΔE_f in Fig. 1. The curves exhibit asymmetry, leaning towards the end members with the smaller cations, as in (Adjaoud et al., 2009; Burton et al., 2006). This phenomonon can be explained by examining the shape of EOS's of the end members. It takes more energy for the structure to contract than to expand by the same amount from the equilibrium volume. Therefore, assuming volume deviations from linearity of random solid solutions are small, as demonstrated above, it pushes the highest point of the ΔE_{vc} curve from x = 0.5 closer to the smaller end member's side. The

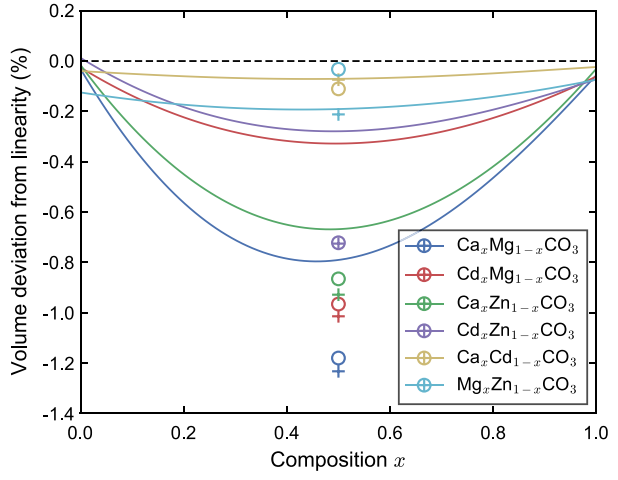

Fig. 5. Volume deviations from linearity for $Ca_{1-x}Mg_xCO_3$, $Cd_{1-x}Mg_xCO_3$, $Ca_{1-x}Zn_xCO_3$, $Cd_{1-x}Zn_xCO_3$, $Ca_{1-x}Cd_xCO_3$ and $Mg_{1-x}Zn_xCO_3$. Curves stand for CE-fitted values of random solid solution configurations. Markers stand for the dolomite structures, with circles for DFT values and crosses for CE-fitted values.

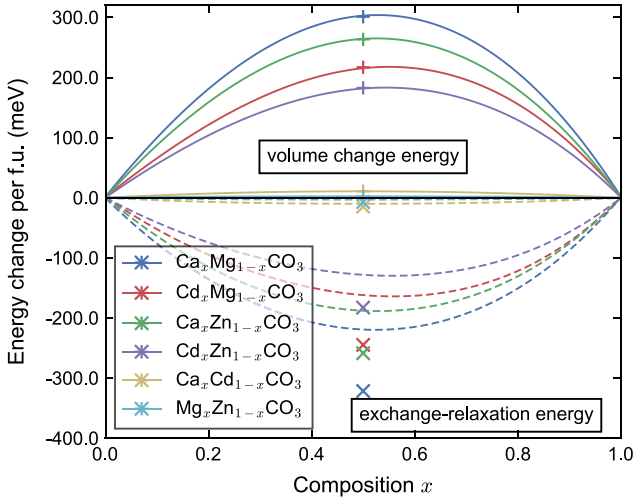

Fig. 6. Volume change and exchange-relaxation energies of $Ca_{1-x}Mg_xCO_3$, $Cd_{1-x}Mg_xCO_3$, $Ca_{1-x}Zn_xCO_3$, $Cd_{1-x}Zn_xCO_3$, $Ca_{1-x}Cd_xCO_3$ and $Mg_{1-x}Zn_xCO_3$. Values are per formula unit, i.e. per exchangeable site. Curves stand for CE-fitted values of random solid solution configurations, with solid above the x-axis for the volume change energies, and dashed below for the exchange-relaxation energies. Markers stand for the dolomite structures, with "+" above and "×" below the x-axis.

outcome is that it takes more energy to substitute a smaller ion with a larger one than vice versa.

In addition, the small difference between the volumes of the ordered dolomite structure and the corresponding random solid solution is negligible when it comes to ΔE_{vc}, but difference of the atomic arrangements plays a major role in ΔE_{xc-rlx}, which explains the energetic difference between them; i.e. the dolomite structure is more favorable than the random solid solution. This is in agreement with a study by Chan and Zunger (Chan and Zunger, 2009) on the step-wise energy changes of random solid solution $Ca_{0.5}Mg_{0.5}CO_3$ and dolomite $CaMg(CO_3)_2$. They made finer division of steps, and stated that the internal relaxation of carbonate systems compensates for the volume mismatch, leading to the energetic stabilization of the solution. The dolomite structure is even more favorable because the CO_3^{2-} anion groups are not distorted, as they are in random solid solutions. The energetic advantage for stability of these dolomite structures is further explored in Section 3.5, by studying various bonds and octahedral distortions, in comparison with their respective end member carbonates.

3.5. Structural analysis

Here we study the lengths (d) of various bonds and angles of MO_6 octahedra (α_{oct}) in $CaCO_3$, $CdCO_3$, $MgCO_3$, $ZnCO_3$ and the six dolomite structures. Values are listed in Table 4. α_{oct} is defined as the O-M-O angle approximately along the trigonal [111] direction. For these carbonates, all values of α_{oct} are slightly above 90°. Differences of bond lengths (Δd) and angles ($\Delta\alpha_{oct}$) in the dolomite structures are also given. These are defined differently for different bonds, following,

$$\begin{aligned}
&\Delta d(\text{C-O}) = d(\text{C-O in dolomite}) - \tfrac{1}{2}\, d\left(\text{C-O in } M^A CO_3\right) - \tfrac{1}{2}\, d\left(\text{C-O in } M^B CO3\right),\\
&\Delta d\left(M^A\text{-}M^B\right) = d\left(M^A\text{-}M^B \text{ in dolomite}\right) - \tfrac{1}{2}\, d\left(M\text{-}M \text{ in } M^A CO_3\right) - \tfrac{1}{2}\, d\left(M\text{-}M \text{ in } M^B CO_3\right),\\
&\Delta d\left(M^i\text{-O}\right) = d\left(M^i\text{-O in dolomite}\right) - d\left(M\text{-O in } M^i CO_3\right),\\
&\Delta\alpha_{oct}\left(M^i\right) = \alpha_{oct}\left(M^i \text{ in dolomite}\right) - \alpha_{oct}\left(M \text{ in } M^i CO_3\right),
\end{aligned} \tag{4}$$

where M is the metal in M^iCO_3 ($i = A, B$) for ease of listing.

Table 4
Various bond lengths (d) and angles of MO_6 octahedra (α_{oct}) in CaCO3, $CdCO_3$, $MgCO_3$, $ZnCO_3$, and the six dolomite structures. M stands for the metal element, and M^A, M^B stand for the first and second metal elements in the dolomite structures. Differences of the two quantities in the dolomite structures from those in the end members are also given. (See main text for definition of differences.)

	d (Å)			α_{oct} (°)	
	C-O	M-M	M-O	M	
$CaCO_3$	1.300	4.097	2.388	92.55	92.43[a]
$CdCO_3$	1.299	4.007	2.339	91.74	
$MgCO_3$	1.297	3.703	2.126	91.90	91.75[a]
$ZnCO_3$	1.298	3.726	2.144	91.70	91.54[a]

	C-O	M^A-M^B	M^A-O	M^B-O	M^A	M^B
$CaMg(CO_3)_2$	1.298	3.893	2.408	2.109	92.70	91.45
$CdMg(CO_3)_2$	1.298	3.846	2.358	2.108	91.83	91.15
$CaZn(CO_3)_2$	1.299	3.908	2.389	2.140	93.48	91.24
$CdZn(CO_3)_2$	1.299	3.865	2.345	2.138	92.38	91.00
$CaCd(CO_3)_2$	1.299	4.049	2.380	2.348	92.67	91.29
$MgZn(CO_3)_2$	1.297	3.712	2.116	2.152	91.93	91.57

Difference from end members						
	C-O	M^A-M^B	M^A-O	M^B-O	M^A	M^B
$CaMg(CO_3)_2$	0.000	−0.007	0.020	−0.017	0.15	−0.45
$CdMg(CO_3)_2$	0.000	−0.009	0.018	−0.017	0.09	−0.75
$CaZn(CO_3)_2$	0.000	−0.004	0.002	−0.004	0.93	−0.46
$CdZn(CO_3)_2$	0.000	−0.002	0.006	−0.006	0.64	−0.70
$CaCd(CO_3)_2$	0.000	−0.003	−0.007	0.008	0.12	−0.45
$MgZn(CO_3)_2$	0.000	−0.003	−0.010	0.009	0.03	−0.13

[a] (Rosenberg and Foit, 1979).

Values of d for the C—O bonds show no change, and minimal changes for M^A-M^B, M^A-O and M^B-O. This is also in agreement with the statement of Chan and Zunger (Chan and Zunger, 2009), that solid solution structures with anion groups rather than single atoms have more internal degrees of freedom to let the atoms adjust to their optimal positions to facilitate optimal bonding, close to their end member chemical environments, hence the minimal changes in values of d. In addition, among all six dolomite structures, $CaMg(CO_3)_2$ and $CdMg(CO_3)_2$ exhibit the largest changes in M^A-M^B, M^A-O and M^B-O, twice or more than the rest, echoing the largest magnitude of ΔE_f (highest stability) in Table 1. It appears that these small adjustments are essential to stabilizing the dolomite structures.

The high correlation between experimental results of MO_6 octahedral distortion and ΔE_f discussed by Rosenberg and Foit (Rosenberg and Foit, 1979) is also observed here. There is a consistent overestimation of ~0.15° relative to the tabulated data (Rosenberg and Foit, 1979). Assuming $MgCO_3$ represents an ideal configuration, α_{oct} of $ZnCO_3$ deviates from that of $MgCO_3$ by −0.20°. Therefore dolomite structures with Zn^{2+} are less stable than their Mg^{2+} counterparts. In addition, mentioned but omitted in the consideration of energetics is the influence of the smaller cation's octahedral distortion on the larger cation's in the dolomite structure. This can be seen from the differences of α_{oct} values of the dolomite structures relative to their end members. In $CaMg(CO_3)_2$ and $CdMg(CO_3)_2$ the octahedral distortions of the smaller cation Mg^{2+} are reduced, by −0.45° and −0.75°, respectively, and those of the larger cations Ca^{2+} and Cd^{2+} are slightly increased, by 0.15° and 0.09°, respectively. However, in $CaZn(CO_3)_2$ and $CdZn(CO_3)_2$, the distortions of the smaller cation Zn^{2+} are reduced by about the same amount, but those of Ca^{2+} and Cd^{2+} are substantially increased, by 0.93° and 0.64°, respectively. The inclusion of Zn^{2+} is therefore more problematic because Ca^{2+} and Cd^{2+} have ionic radii close to the maximum that can be tolerated in octahedral coordination (Rosenberg and Foit, 1979).

4. Conclusion

We performed first-principles phase diagram calculations for the four quasibinary carbonate systems $Ca_{1-x}Zn_xCO_3$, $Cd_{1-x}Zn_xCO_3$, $Ca_{1-x}Cd_xCO_3$ and $Mg_{1-x}Zn_xCO_3$ ($0 \le x \le 1$) with DFT, CE and MC simulations. The end members and the dolomite structures were individually studied to analyze their structural parameters and bonding characteristics. Consolute temperatures and continuous order-disorder transition temperatures are 1450 K for $Ca_{1-x}Zn_xCO_3$ and 1000 K for $Cd_{1-x}Zn_xCO_3$, but below 100 K for $Ca_{1-x}Cd_xCO_3$ and $Mg_{1-x}Zn_xCO_3$. In agreement with existing literature, consolute temperatures increase with increasing differences in cation radii. If dolomite structures are assumed to be stable, they persist to 1150 K for $Ca_{1-x}Zn_xCO_3$, and 900 K for $Cd_{1-x}Zn_xCO_3$ before decomposition at peritectoid points. This confirms the conjectured phase diagram for $Ca_{1-x}Zn_xCO_3$ (Goldsmith, 1983). In addition, ΔE_f of the dolomite structures were decomposed into two parts: first a volume change, then chemical exchange and relaxation. They were compared with their corresponding random solid solutions at the same bulk compositions. (Meta)stability of the dolomite structures was demonstrated by this division of energy, and was also studied by examining the bond lengths and cation octahedral distortions.

Acknowledgements

The computing for this project was performed at the Tandy Supercomputing Center and Ohio Supercomputer Center (OSC) (Ohio-Supercomputer-Center, 1987). We thank the National Science Foundation grant CMMI 1234777 and 1629239 for funding this work.

Appendix A. Supplementary data

Supplementary data to this article can be found online at http://dx.doi.org/10.1016/j.chemgeo.2016.09.024.

References

Adjaoud, O., Steinle-Neumann, G., Burton, B.P., van de Walle, A., 2009. First-principles phase diagram calculations for the HfC–TiC, ZrC–TiC, and HfC–ZrC solid solutions. Phys. Rev. B 80, 134112. http://dx.doi.org/10.1103/PhysRevB.80.134112.

Anovitz, L.M., Essene, E.J., 1987. Phase equilibria in the system $CaCO_3$-$MgCO_3$-$FeCO_3$. J. Petrol. 28, 389–415. http://dx.doi.org/10.1093/petrology/28.2.389.

Barabash, S.V., Chepulskii, R.V., Blum, V., Zunger, A., 2009. First-principles determination of low-temperature order and ground states of Fe-Ni, Fe-Pd, and Fe-Pt. Phys. Rev. B 80, 220201. http://dx.doi.org/10.1103/PhysRevB.80.220201.

Binder, K., Heermann, D.W., 1988. Monte Carlo Simulation in Statistical Physics. Springer-Verlag, New York.

Birch, F., 1947. Finite elastic strain of cubic crystals. Phys. Rev. 71, 809–824.

Birch, W.D., 1983. Zincian dolomite from broken hill, New South Wales. J. Geol. Soc. Aust. 30, 85–87. http://dx.doi.org/10.1080/00167618308729238.

Blöchl, P.E., 1994. Projector augmented-wave method. Phys. Rev. B 50, 17953–17979. http://dx.doi.org/10.1103/PhysRevB.50.17953.

Boni, M., Mondillo, N., Balassone, G., 2011. Zincian dolomite: a peculiar dedolomitization case? Geology 39, 183–186. http://dx.doi.org/10.1130/G31486.1.

Burton, B.P., van de Walle, A., 2003. First-principles-based calculations of the $CaCO_3$-$MgCO_3$ and $CdCO_3$-$MgCO_3$ subsolidus phase diagrams. Phys. Chem. Miner. 30, 88–97. http://dx.doi.org/10.1007/s00269-002-0294-y.

Burton, B.P., van de Walle, A., 2006. First-principles phase diagram calculations for the system NaCl-KCl: the role of excess vibrational entropy. Chem. Geol. 225, 222–229. http://dx.doi.org/10.1016/J.Chemgeo.2005.08.016.

Burton, B.P., van de Walle, A., 2012a. First principles phase diagram calculations for the octahedral-interstitial system αTiOX, 0 ≤ X ≤ 1/2. Calphad 39, 97–103. http://dx.doi.org/10.1016/j.calphad.2012.09.004.

Burton, B.P., van de Walle, A., 2012b. First principles phase diagram calculations for the octahedral-interstitial system HfOX, 0 ≤ X ≤ 1/2. Calphad 37, 151–157. http://dx.doi.org/10.1016/j.calphad.2011.12.011.

Burton, B.P., van de Walle, A., Kattner, U., 2006. First principles phase diagram calculations for the wurtzite-structure systems AlN–GaN, GaN–InN, and AlN–InN. J. Appl. Phys. 100, 113528. http://dx.doi.org/10.1063/1.2372309.

Burton, B.P., Demers, S., van de Walle, A., 2011. First principles phase diagram calculations for the wurtzite-structure quasibinary systems SiC-AlN, SiC-GaN and SiC-InN. J. Appl. Phys. 110, 023507. http://dx.doi.org/10.1063/1.3602149.

Burton, B.P., van de Walle, A., Stokes, H.T., 2012. First principles phase diagram calculations for the octahedral-interstitial system ZrOX, 0 ≤ X ≤ 1/2. J. Phys. Soc. Jpn. 81, 014004. http://dx.doi.org/10.1143/JPSJ.81.014004.

Capobianco, C., Burton, B.P., Davidson, P.M., Navrotsky, A., 1987. Structural and calorimetric studies of order-disorder in $CdMg(CO_3)_2$. J. Solid State Chem. 71, 214–223. http://dx.doi.org/10.1016/0022-4596(87)90161-7.

Chan, J.A., Zunger, A., 2009. II-VI oxides phase separate whereas the corresponding carbonates order: the stabilizing role of anionic groups. Phys. Rev. B 80, 165201. http://dx.doi.org/10.1103/PhysRevB.80.165201.

Chen, W.Z., Xu, G.L., Martin-Bragado, I., Cui, Y.W., 2015. Non-empirical phase equilibria in the Cr-Mo system: a combination of first-principles calculations, cluster expansion and Monte Carlo simulations. Solid State Sci. 41, 19–24. http://dx.doi.org/10.1016/j.solidstatesciences.2015.01.012.

Connolly, J.W.D., Williams, A.R., 1983. Density-functional theory applied to phase-transformations in transition-metal alloys. Phys. Rev. B 27, 5169–5172. http://dx.doi.org/10.1103/PhysRevB.27.5169.

de Capitani, C., Peters, T., 1981. The solvus in the system $MnCO_3$-$CaCO_3$. Contrib. Mineral. Petrol. 76, 394–400. http://dx.doi.org/10.1007/BF00371481.

De Fontaine, D., 1994. Cluster approach to order-disorder transformations in alloys. Solid State Phys. - Adv. Res. Appl. 47 (47), 33–176.

Ducastelle, F., 1991. Order and Phase Stability in Alloys. Elsevier Science, New York.

Dunweg, B., Landau, D.P., 1993. Phase-diagram and critical-behavior of the Si-Ge unmixing transition - a Monte-Carlo study of a model with elastic degrees of freedom. Phys. Rev. B 48, 14182–14197. http://dx.doi.org/10.1103/Physrevb.48.14182.

Gao, M.C., Suzuki, Y., Schweiger, H., Dogan, O.N., Hawk, J., Widom, M., 2013. Phase stability and elastic properties of Cr-V alloys. J. Physics-Condensed Matter 25, 075402. http://dx.doi.org/10.1088/0953-8984/25/7/075402.

Ghosh, G., van de Walle, A., Asta, M., 2008. First-principles calculations of the structural and thermodynamic properties of bcc, fcc and hcp solid solutions in the Al–TM (TM = Ti, Zr and Hf) systems: a comparison of cluster expansion and supercell methods. Acta Mater. 56, 3202–3221. http://dx.doi.org/10.1016/j.actamat.2008.03.006.

Gilg, H.A., Boni, M., Hochleitner, R., Struck, U., 2008. Stable isotope geochemistry of carbonate minerals in supergene oxidation zones of Zn–Pb deposits. Ore Geol. Rev. 33, 117–133. http://dx.doi.org/10.1016/j.oregeorev.2007.02.005.

Goldsmith, J.R., 1972. Cadmium dolomite and the system $CdCO_3$-$MgCO_3$. J. Geol. 80, 617–626.

Goldsmith, J.R., 1983. Phase relations of rhombohedral carbonates. Rev. Mineral. Geochem. 11, 49–76.

Goldsmith, J.R., Graf, D.L., 1958. Structural and compositional variations in some natural dolomites. J. Geol. 66, 678–693.

Goldsmith, J.R., Graf, D.L., 1960. Subsolidus relations in the system $CaCO_3$-$MgCO_3$-$MnCO_3$. J. Geol. 68, 324–335.

Goldsmith, J.R., Northrop, D.A., 1965. Subsolidus phase relations in the systems $CaCO_3$ — $MgCO_3$ — $CoCO_3$ and $CaCO_3$ — $MgCO_3$ — $NiCO_3$. J. Geol. 73, 817–829.

Goldsmith, J.R., Graf, D.L., Witters, J., Northrop, D.A., 1962. Studies in the system $CaCO_3$-$MgCO_3$-$FeCO_3$: 1. Phase relations; 2. A method for major-element spectrochemical analysis; 3. compositions of some ferroan dolomites. J. Geol. 70, 659–688. http://dx.doi.org/10.1086/626865.

Graf, D.L., 1961. Crystallographic tables for the rhombohedral carbonates. Am. Mineral. 46, 1283–1316.

Khan, M.R., Barber, D.J., 1990. Composition-related microstructures in zinc-bearing carbonate assemblages from Broken Hill, New South Wales. Mineral. Petrol. 41, 229–245. http://dx.doi.org/10.1007/BF01168497.

Klein, C., Hurlbut, C.S., Dana, J.D., 1993. Manual of Mineralogy. Wiley.

Kohan, A.F., Tepesch, P.D., Ceder, G., Wolverton, C., 1998. Computation of alloy phase diagrams at low temperatures. Comput. Mater. Sci. 9, 389–396. http://dx.doi.org/10.1016/S0927-0256(97)00168-7.

Kresse, G., Furthmuller, J., 1996a. Efficiency of ab-initio total energy calculations for metals and semiconductors using a plane-wave basis set. Comput. Mater. Sci. 6, 15–50. http://dx.doi.org/10.1016/0927-0256(96)00008-0.

Kresse, G., Furthmuller, J., 1996b. Efficient iterative schemes for ab initio total-energy calculations using a plane-wave basis set. Phys. Rev. B 54, 11169–11186. http://dx.doi.org/10.1103/PhysRevB.54.11169.

Kresse, G., Hafner, J., 1993. Ab initio molecular dynamics for liquid metals. Phys. Rev. B 47, 558–561.

Kresse, G., Hafner, J., 1994. Ab initio molecular-dynamics simulation of the liquid-metal–amorphous-semiconductor transition in germanium. Phys. Rev. B 49, 14251–14269. http://dx.doi.org/10.1103/PhysRevB.49.14251.

Kresse, G., Joubert, D., 1999. From ultrasoft pseudopotentials to the projector augmented-wave method. Phys. Rev. B 59, 1758–1775. http://dx.doi.org/10.1103/PhysRevB.59.1758.

Kumagai, Y., Soda, Y., Oba, F., Seko, A., Tanaka, I., 2012. First-principles calculations of the phase diagrams and band gaps in $CuInSe_2$ - $CuGaSe_2$ and $CuInSe_2$ -$CuAlSe_2$ pseudobinary systems. Phys. Rev. B 85, 033203. http://dx.doi.org/10.1103/PhysRevB.85.033203.

Laks, D.B., Ferreira, L.G., Froyen, S., Zunger, A., 1992. Efficient cluster-expansion for substitutional systems. Phys. Rev. B 46, 12587–12605. http://dx.doi.org/10.1103/PhysRevB.46.12587.

Lamble, G.M., Reeder, R.J., Northrup, P.A., 1997. Characterization of heavy metal incorporation in calcite by XAFS spectroscopy. Le J. Phys. IV 7. http://dx.doi.org/10.1051/jp4:1997238 C2-793–C2-797.

Laradji, M., Landau, D.P., Dunweg, B., 1995. Structural-properties of Si1-xGex alloys - a Monte-Carlo simulation with the Stillinger-Weber potential. Phys. Rev. B 51, 4894–4902. http://dx.doi.org/10.1103/Physrevb.51.4894.

Li, X.K., Xue, H.T., Tang, F.L., Lu, W.J., 2015. First-principles calculation of sulfur-selenium segregation in ZnSe1-xSx: the role of lattice vibration. Mater. Sci. Semicond. Process. 39, 96–102. http://dx.doi.org/10.1016/j.mssp.2015.03.024.

Liu, J.Z., Zunger, A., 2009. Thermodynamic theory of epitaxial alloys: first-principles mixed-basis cluster expansion of (In, Ga)N alloy film. J. Phys. Condens. Matter 21, 295402. http://dx.doi.org/10.1088/0953-8984/21/29/295402.

Liu, J.Z., van de Walle, A., Ghosh, G., Asta, M., 2005. Structure, energetics, and mechanical stability of Fe-Cu bcc alloys from first-principles calculations. Phys. Rev. B 72, 144109. http://dx.doi.org/10.1103/PhysRevB.72.144109.

Liu, Z.T.Y., Gall, D., Khare, S.V., 2014a. Electronic and bonding analysis of hardness in pyrite-type transition-metal pernitrides. Phys. Rev. B 90, 134102.

Liu, Z.T.Y., Zhou, X., Gall, D., Khare, S.V., 2014b. First-principles investigation of the structural, mechanical and electronic properties of the NbO-structured 3d, 4d and 5d transition metal nitrides. Comput. Mater. Sci. 84, 365–373. http://dx.doi.org/10.1016/j.commatsci.2013.12.038.

Liu, Z.T.Y., Zhou, X., Khare, S.V., Gall, D., 2014c. Structural, mechanical and electronic properties of 3d transition metal nitrides in cubic zincblende, rocksalt and cesium chloride structures: a first-principles investigation. J. Physics-Condensed Matter 26, 25404. http://dx.doi.org/10.1088/0953-8984/26/2/025404.

Liu, X., Lu, X., Liu, X., Zhou, H., 2015. Atomistic simulation on mixing thermodynamics of calcite-smithsonite solid solutions. Am. Mineral. 100, 172–180. http://dx.doi.org/10.2138/am-2015-4815.

Mondillo, N., Boni, M., Balassone, G., Grist, B., 2011. In search of the lost zinc: A lesson from the Jabali (Yemen) nonsulfide zinc deposit. J. Geochem. Explor. 108, 209–219. http://dx.doi.org/10.1016/j.gexplo.2011.02.010.

Navrotsky, A., Capobianco, C., 1987. Enthalpies of formation of dolomite and of magnesian calcites. Am. Mineral. 72, 782–787.

Newman, M.E.J., Barkema, G.T., 1999. Monte Carlo Methods in Statistical Physics. Clarendon Press, Oxford.

Ohio-Supercomputer-Center, 1987. Ohio Supercomputer Center [WWW Document]. http://osc.edu/ark:/19495/f5s1ph73.

Perdew, J.P., Chevary, J.A., Vosko, S.H., Jackson, K.A., Pederson, M.R., Singh, D.J., Fiolhais, C., 1992. Atoms, molecules, solids, and surfaces: applications of the generalized gradient approximation for exchange and correlation. Phys. Rev. B 46, 6671–6687. http://dx.doi.org/10.1103/PhysRevB.46.6671.

Perdew, J.P., Chevary, J.A., Vosko, S.H., Jackson, K.A., Pederson, M.R., Singh, D.J., Fiolhais, C., 1993. Atoms, molecules, solids, and surfaces - applications of the generalized gradient approximation for exchange and correlation (Vol 46, Pg 6671, 1992). Phys. Rev. B 48, 4978. http://dx.doi.org/10.1103/Physrevb.48.4978.2.

Powell, R., Condliffe, D.M., Condliffe, E., 1984. Calcite-dolomite geothermometry in the system $CaCO_3$-$MgCO_3$-$FeCO_3$: an experimental study. J. Metamorph. Geol. 2, 33–41. http://dx.doi.org/10.1111/j.1525-1314.1984.tb00283.x.

Purton, J.A., Allan, N.L., Lavrentiev, M.Y., Todorov, I.T., Freeman, C.L., 2006. Computer simulation of mineral solid solutions. Chem. Geol. 225, 176–188. http://dx.doi.org/10.1016/j.chemgeo.2005.08.032.

Ravi, C., Panigrahi, B.K., Valsakumar, M.C., van de Walle, A., 2012. First-principles calculation of phase equilibrium of V-Nb, V-Ta, and Nb-Ta alloys. Phys. Rev. B 85, 054202. http://dx.doi.org/10.1103/PhysRevB.85.054202.

Reeder, R.J., Lamble, G.M., Northrup, P.A., 1999. XAFS study of the coordination and local relaxation around Co_2+, Zn_2+, Pb_2+, and Ba_2+ trace elements in calcite. Am. Mineral. 84, 1049–1060. http://dx.doi.org/10.2138/am-1999-7-807.

Rosenberg, P.E., 1963a. Synthetic solid solutions in systems $MgCO_3$-$FeCO_3$ and $MnCO_3$-$FeCO_3$. Am. Mineral. 48, 1396.

Rosenberg, P.E., 1963b. Subsolidus relations in the system $CaCO_3$-$FeCO_3$. Am. J. Sci. 261, 683–689. http://dx.doi.org/10.2475/ajs.261.7.683.

Rosenberg, P.E., 1967. Subsolidus relations in the system $CaCO_3$-$MgCO_3$-$FeCO_3$ between 350 and 550 °C. Am. Mineral. 52, 787–796.

Rosenberg, P.E., Champness, P.E., 1989. Zincian dolomites and associated carbonates from the Warynski mine, Poland: an AEM investigation. Am. Mineral. 74, 461–465.

Rosenberg, P.E., Foit, F.F., 1979. The stability of transition metal dolomites in carbonate systems: a discussion. Geochim. Cosmochim. Acta 43, 951–955. http://dx.doi.org/10.1016/0016-7037(79)90085-1.

Sanchez, J.M., Ducastelle, F., Gratias, D., 1984. Generalized cluster description of multicomponent systems. Physica A 128, 334–350. http://dx.doi.org/10.1016/0378-4371(84)90096-7.

Tsusue, A., Holland, H.D., 1966. The coprecipitation of cations with $CaCO_3$-III. The coprecipitation of Zn_2+ with calcite between 50 and 250 °C. Geochim. Cosmochim. Acta 30, 439–453. http://dx.doi.org/10.1016/0016-7037(66)90072-X.

Usanmaz, D., Nath, P., Plata, J.J., Hart, G.L.W., Takeuchi, I., Nardelli, M.B., Fornari, M., Curtarolo, S., 2015. First principles thermodynamical modeling of the binodal and spinodal curves in lead chalcogenides. Phys. Chem. Chem. Phys. 18, 5005–5011. http://dx.doi.org/10.1039/C5CP06891F.

van de Walle, A., 2009. Multicomponent multisublattice alloys, nonconfigurational entropy and other additions to the Alloy Theoretic Automated Toolkit. Calphad 33, 266–278. http://dx.doi.org/10.1016/J.Calphad.2008.12.005.

van de Walle, A., 2013. Methods for first-principles alloy thermodynamics. JOM J. Miner. Met. Mater. Soc. 65, 1523–1532. http://dx.doi.org/10.1007/S11837-013-0764-3.

van de Walle, A., Asta, M., 2002. Self-driven lattice-model Monte Carlo simulations of alloy thermodynamic properties and phase diagrams. Model. Simul. Mater. Sci. Eng. 10, 521–538.

van de Walle, A., Ceder, G., 2002a. Automating first-principles phase diagram calculations. J. Phase Equilibria 23, 348–359.

van de Walle, A., Ceder, G., 2002b. The effect of lattice vibrations on substitutional alloy thermodynamics. Rev. Mod. Phys. 74, 11–45. http://dx.doi.org/10.1103/Revmodphys.74.11.

van de Walle, A., Asta, M., Ceder, G., 2002. The Alloy Theoretic Automated Toolkit: a user guide. Calphad-Computer Coupling Phase Diagrams Thermochem. 26, 539–553. http://dx.doi.org/10.1016/S0364-5916(02)80006-2.

van de Walle, A., Moser, Z., Gasior, W., 2004. First-principles calculation of the Cu-Li phase diagram. Arch. Metall. Mater. 49, 535–544.

van de Walle, A., Tiwary, P., de Jong, M., Olmsted, D.L., Asta, M., Dick, A., Shin, D., Wang, Y., Chen, L.Q., Liu, Z.K., 2013. Efficient stochastic generation of special quasirandom structures. Calphad-Computer Coupling Phase Diagrams Thermochem. 42, 13–18. http://dx.doi.org/10.1016/J.Calphad.2013.06.006.

Vinograd, V.L., Winkler, B., Putnis, A., Gale, J.D., Sluiter, M.H.F., 2006. Static lattice energy calculations of mixing and ordering enthalpy in binary carbonate solid solutions. Chem. Geol. 225, 304–313. http://dx.doi.org/10.1016/j.chemgeo.2005.08.023.

Vinograd, V.L., Burton, B.P., Gale, J.D., Allan, N.L., Winkler, B., 2007. Activity–composition relations in the system $CaCO_3$–$MgCO_3$ predicted from static structure energy calculations and Monte Carlo simulations. Geochim. Cosmochim. Acta 71, 974–983. http://dx.doi.org/10.1016/j.gca.2006.11.008.

Vinograd, V.L., Sluiter, M.H.F., Winkler, B., 2009. Subsolidus phase relations in the $CaCO_3$–$MgCO_3$ system predicted from the excess enthalpies of supercell structures with single and double defects. Phys. Rev. B 79, 104201. http://dx.doi.org/10.1103/PhysRevB.79.104201.

Wang, Q., de Leeuw, N.H., 2008. A computer-modelling study of $CdCO_3$-$CaCO_3$ solid solutions. Mineral. Mag. 72, 525–529. http://dx.doi.org/10.1180/minmag.2008.072.1.525.

Wang, Q., Grau-Crespo, R., De Leeuw, N.H., 2011. Mixing thermodynamics of the calcite-structured $(Mn,Ca)CO_3$ solid solution: a computer simulation study. J. Phys. Chem. B 115, 13854–13861. http://dx.doi.org/10.1021/jp200378q.

Wang, Y., Liu, Z.T.Y., Khare, S.V., Collins, S.A., Zhang, J., Wang, L., Zhao, Y., 2016. Thermal equation of state of silicon carbide. Appl. Phys. Lett. 108, 61906. http://dx.doi.org/10.1063/1.4941797.

Xue, H.T., Tang, F.L., Li, X.K., Wan, F.C., Lu, W.J., Rui, Z.Y., Feng, Y.D., 2014. Phase equilibrium of a $CuInSe_2$-$CuInS_2$ pseudobinary system studied by combined first-principles calculations and cluster expansion Monte Carlo simulations. Mater. Sci. Semicond. Process. 25, 251–257. http://dx.doi.org/10.1016/j.mssp.2013.12.021.

Zhang, J.Z., Reeder, R.J., 1999. Comparative compressibilities of calcite-structure carbonates: Deviations from empirical relations. Am. Mineral. 84, 861–870.

Zunger, A., 1994. First principles statistical mechanics of semiconductor alloys and intermetallic compounds. In: Turchi, P.E., Gonis, A. (Eds.), NATO ASI on Statics and Dynamics of Alloy Phase Transformation. Plenum Press, New York, p. 361.